Towards Automated Modelling of Maxillofacial Musculature

G. D. Parker[1,2], N. Drage[3,4], P. L. Rosin[2], A. D. Marshall[2], S. Richmond[4], J. Evans[1], and D. K. Jones[1]
[1]CUBRIC, School of Psychology, Cardiff University, Cardiff, United Kingdom, [2]School of Computer Science, Cardiff University, Cardiff, United Kingdom, [3]Cardiff Vale NHS Trust, United Kingdom, [4]School of Dentistry, Cardiff University, United Kingdom

Introduction

Patient-specific models of maxillofacial musculature would be of great use in evaluation of prospective surgical treatment options. Due to complex fibre interactions and low image SNR within this region, both diffusion tensor MRI (DT-MRI [1]) and diffusion spectrum imaging [2] have been precluded from use despite previous application to large muscles (due to inability to resolve crossing fibre [3] and SNR concerns regarding b-value requirements respectively), thus directing our focus towards constrained spherical harmonic deconvolution [4] (CSD). CSD assumes that fibre orientation densities (FOD's) may be derived through deconvolution of an idealised (calibrated) single fibre response function from one fit to the target diffusion weighted signal, yielding information regarding fibre orientations. Current data-driven calibration techniques make assumptions connecting the fractional anisotropy (FA) of a signal to the likelihood that it represents a single fibre, averaging the spherical basis functions of the most anisotropic components of an image (typically 0.8>FA>1 [4]) to derive an idealised response. While such techniques work adequately with highly anisotropic target fibres (e.g. white matter), they are neither directly applicable (producing FOD artefacts when deconvolved from low anisotropy targets, e.g. muscle) nor adaptable (muscle fibre is not unique within its FA range) to maxillofacial use. In this work we propose a novel automated tissue-specific calibration technique and provide preliminary results of unsupervised muscle segmentation through affinity propagation clustering [5].

Materials and Methods

Using a GE 3T HDx system with an 8 channel brain imaging array - images were acquired according to a 60 direction, 6 b0, 450s/mm^2 b-val, 3x3x3mm voxel resolution, TR/TE = 12/103ms protocol. Subsequent CSD (lmax = 8) tracking reconstructions employ a regular 2x2x2mm seed point grid, step size of 0.5mm and termination criteria of 25^o angular deviation or a maximum FOD magnitude below 0.1. Three specific calibration strategies are examined (1) Blind application of a 'conventional' 0.8<FA<1 calibration scheme. (2) Exemplar calibration – highly constrained DT-MRI streamlines (5^o angular threshold ensuring tracking only along straight fibres) are initiated from way points manually positioned across fibrous structures with the desired diffusive properties (ensuring tissue specificity), basis functions from voxels intersected by these streamlines are averaged to generate the response. Samples of the *spinalis capitis* (muscle specific) and spinal cord (moderate FA to aid discussion) are selected as exemplars. (3) Automated calibration – Voxel-wise coherence (Eq 1) is calculated across the image: those voxels demonstrating high coherence (i.e. all voxels within straight fibrous structures) are selected. To obtain tissue-specificity, results are filtered by predetermined mean diffusivity and FA ranges (e.g. MD of muscle ≈ 0.014mm^2/s, approximately twice that of white matter). Basis functions from remaining voxels are averaged to create the fiber response. A coherence threshold of 0.8 (0-1), MD range of $1.43\text{x}10^{-3} \pm 0.49\text{x}10^{-3}$mm^2/s (mean MD over a sample of *masseter* muscle ± one standard deviation) and FA of 0.321 ± 0.13 (again mean *masseter* value ± one SD) were selected. Results are judged by consistency with known anatomy. Initial comparisons focused on simple large structures, i.e. the *masseter* and *temporalis* muscles, as a means of validating general applicability; proceeding to investigation of crossing fibre resolution through reconstructions of the *buccinator* and *risorius* – both of which share roughly orthogonal intersections with the *masseter*.

To assess unsupervised segmentation, manually selected fibre tracts (those representing the *temporalis and masseter* in the case of Fig.1b) are combined to generate model tractography for an anatomical region. Affinity propagation clustering [5]- a technique requiring no *a priori* knowledge of the expected number of clusters - is then applied via the medium of between-tract asymmetric Hausdorff distance measures [6] and outcomes judged by concurrence with manual segmentation.

Results

In general, conventional (FA-based) calibration produces incomplete reconstructions due to premature tract termination in areas of low anisotropy or high curvature. Spinal calibration exhibits similar failings, albeit to a lower degree. Tissue specific calibrations do not possess such artefacts, producing anatomically plausible reconstructions where data quality allows (see discussion). Direct comparison between the two tissue specific calibrations indicates neither possesses a clear advantage. Unsupervised reconstruction successfully delineates the two muscle groups - in that there is no shared membership of any one cluster by the two muscles. However, intriguingly, the cluster-based segmentation also yields sub-divisions within a muscle.

Discussion

As expected, fibre tracking through conventional CSD calibration produces flawed results. A combination of genuine fibre curvature and errors introduced to the FOD through inappropriate calibration produces "between-step" deviations sufficient to exceed the 25^o angular threshold causing the observed premature terminations. Increasing angular thresholds is not a viable solution; the primary effect of CSD miscalibration is the appearance of spurious fibre indications at approximately 55^o, 90^o and 125^o to the correct fibre orientation. Thus, in cases where premature termination has occurred, angles subtended between an artefactual fibre at 55^o and the incoming vector are often lower than those subtended by the true orientation, causing tractography to follow phantom fibre (detailed study is beyond the scope of this work). Progressive improvements from conventional calibration (FA=0.8+) through spinal exemplar (0.48) to muscle-specific calibrations (~0.32) clearly imply a correlation between solution quality and calibration discrepancy (difference between calibration and ideal FA's), reinforcing our assertion that specific calibration is necessary. Additionally, parity between manual and automated calibration indicates that, for the novice user, our fully automated method may provide a suitable "black box" approach to data-driven CSD calibration, ideal for application in the clinical environment. There is still room for improvement in image acquisition to minimize susceptibility-induced distortions adjacent to the mouth, which often prevents complete reconstruction of the *risorius* and *buccinator* muscles (manifesting as premature termination with the cheek). Fortunately however, the regions of interest (contact patches with the *masseter* muscle) are sufficiently intact to permit clear indications of crossing fibre resolution under all calibration methods, highlighting the promise of CSD in this area of research. The ability to delineate muscles through unsupervised means is encouraging. Subdivisions found by the clustering within a muscle may reflect important layering or differences in pennation angle, both of which would provide additional (surgically useful) information. Future work will be undertaken to differentiate between important and trivial subdivisions.

$$C = \frac{\sqrt{6}}{\sqrt{216}+\sqrt{432}+\sqrt{128}} \sum_{n=1}^{26} w(V_t.V_n)$$

$$w = \begin{cases} 1 & \text{if voxels share a face} \\ \frac{1}{\sqrt{2}} & \text{if voxels share an edge} \\ \frac{1}{\sqrt{3}} & \text{if voxels share a vertex} \end{cases}$$

Eq. 1: Normalised weighted sum of dot products between first eigenvectors of target voxels, V_t, and their 26 immediate neighbours V_n.

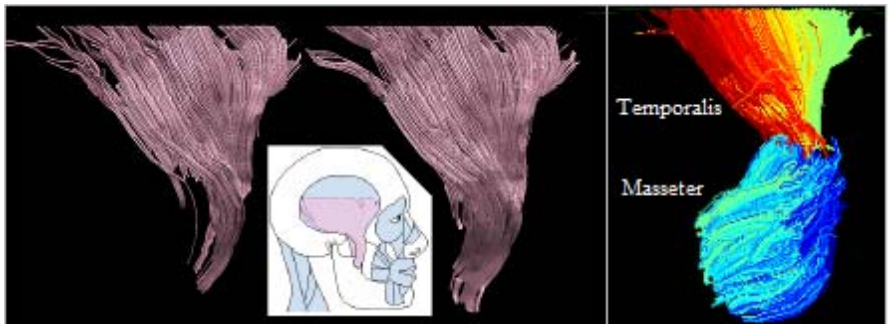

Fig 1a: Left: Spinal exemplar Right: Automated calibration Reconstructions of the *temporalis* muscle. Note the difference between the results in areas of curvature.

Fig 1b: Unsupervised Segmentation Note clusters (colours) are not shared between muscles

[1]Pierpaoli and Basser (1996) MRM 36:893-906 [2]Gilbert *et al* (2006) The Anatomical Record 288A:1173- 1182 [3]Alexander *et al.* (2001) MRM 45(5):770-780 [4]Tournier *et al.* 2004. Neuroimage 23:1176-1185. [5]Frey and Dueck. 2007.Science 315:972-976 [6]Leemans and Jones. 2009.ISMRM-17 Hawaii. p.855.